P H Y S I C A L   R E V I E W   L E T T E R S

Hidden Stochastic Nature of a Single Bacterial Motor

Ekaterina A. Korobkova, Thierry Emonet, Heungwon Park, and Philippe Cluzel

*The Institute for Biophysical Dynamics, The James Franck Institute, The University of Chicago, 56540 South Ellis Avenue,
Chicago, Illinois 60637, USA*

The rotary flagellar motor of Escherichia coli bacterium switches stochastically between the clockwise (CW) and counterclockwise (CCW) direction. We found that the CW and CCW intervals could be described by a gamma distribution, suggesting the existence of hidden Markov steps preceding each motor switch. Power spectra of time series of switching events exhibited a peaking frequency instead of the Lorentzian profile expected from standard kinetic two-state models. Our analysis indicates that the number of hidden steps may be a key dynamical parameter underlying the switching process in a single bacterial motor as well as in large cooperative molecular systems.

Introduction.—The bacterium of *E. coli* is propelled by several flagella and the rotation of each flagellum is controlled by a rotary motor [1]. When motors rotate counterclockwise (CCW), the flagella bundle together and the bacterium swims smoothly; when motors rotate clockwise (CW), the bundle breaks apart and the bacterium tumbles in a random fashion. The modulation of the tumbling frequency allows bacteria to perform chemotaxis by swimming toward attractant or away from repellent. Single cell experiments established that the CW bias (probability that a motor spins CW) increases nonlinearly, in a sigmoidal fashion, with the concentration of the active form, CheY-P, of the signaling molecule [2,3]. The steep input-output relationship of the motor is associated with an underlying allosteric process catalyzed by the binding of the signaling CheY-P molecules to the basal part of the motor [4]. CheY-P molecules interact with a ring shape assembly of about 34 identical FliM protein subunits. For several decades, a series of models have aimed to identify the underlying general kinetic parameters that control the steady states behavior of motor switches [4–9]. Recently, Tu and Grinstein [10] theoretically showed, in agreement with recent experiments [11,12], that in a dynamical two-state (CW and CCW) model the temporal fluctuation of CheY-P drives, at long time scales, the switching behavior of the motor to produce a power-law distribution for the durations of the CCW states. Bialek *et al.* [5] used the bacterial motor as a model system to evaluate the noise limitation of intracellular signaling. More specifically, Duke *et al.* [4,13] presented a unified stochastic approach demonstrating that all allosteric switches could be mapped to a simple one-dimensional Ising model. In particular, this stochastic approach to cooperative molecular behavior was used to describe how the equilibrium between the CCW and CW states of the bacterial motor depends nonlinearly on the concentration of CheY-P. It was hypothesized that each subunit may undergo a conformational change catalyzed by the binding of CheY-P. The coupling between neighboring subunits favors the propagation of conformational

change of subunits along the ring. Although this model reproduces satisfactorily the equilibrium behavior, very little is still known about the underlying dynamical behavior of such cooperative switching. In this Letter, we measure and analyze long binary time series of switching events from individual motors to characterize experimentally the underlying stochastic nature of this classic allosteric system at the level of a single motor.

Experimental conditions.—Switching behavior of individual motors in wild-type cells was already reported in earlier studies [14]. In wild-type cells the chemotaxis network that controls the concentration of the input signal of the motor can introduce some noise as reported in [11,15]. In order to study the stochastic nature of the motor alone without the contribution of the network, we used the PS2001 bacterial strain whose chemotaxis network was defective [9]. We also used the activated CheY* mutant protein (CheYD13K), which does not need to be phosphorylated in order to bind to the motor. Thus, in our experiment, the concentration of the CheY* that binds to the subunits of the ring is not controlled by the chemotaxis network but stably preexpressed from an inducible vector expressing the CheYD13K gene [11]. Under these conditions the concentration of CheY* does not exhibit temporal correlation at long time scales as described in [10,11]. We analyzed the distributions of CCW and CW events of a bacterial motor at the different preinduction levels of CheY*. We recorded the motor switching events from a bacterial motor using the same apparatus as in [11]. We immobilized the cells on a glass surface and used $0.5 \ \mu$m latex beads to label and visualize some rotating flagella [2,11,12]. By contrast with tethered assays like in [15], motors never stop rotating and exhibit only CW and CCW rotational states. We used a sampling rate of 100 Hz and the resolution time was about 0.1 sec. We represent the motor switches with a binary time series (CCW and CW states). We varied the intracellular concentration [CheY*] by preinducing the cells with various amounts of isopropyl-β-D-thiogalactoside, [IPTG]. PS2001 mutant

058105-1

cells were grown from an overnight culture in tryp-tone broth at 30 C with various IPTG concentrations (with [IPTG] = 25–100 μM) and then harvested (optical density = 0.5 at 595 nm). Cells were then washed and suspended in minimal medium [7.6 mM (NH4)2 SO4, 2 mM MgSO4, 20 μM FeSO4, 0.1 mM EDTA, 0.1 mM L-methionine, 60 mM potassium phosphate pH 6.8]. CheYD13K was expressed from an inducible lac promoter pMS164 [9]. PS2001 strain is deleted for CheB, CheZ, and CheY. The resulting CW bias varies from 0 to 1 for cells for different IPTG levels. We sorted the binary time series by CW bias into the following 9 intervals: 0.1 ± 0.05; 0.2 ± 0.05; ...; 0.9 ± 0.05. Data from each bin came from ten different cells with a typical total observation time of 15 minutes each. This binning procedure was crucial to our study because it allowed us to analyze the noise from individual motors that have about the same [CheY*]. In previous studies [6,9,14] data from cells possibly with large difference in [CheY*] were combined together, which masked the dynamical properties of the cooperative switching in a single motor.

CW and CCW interval distributions.—Information about the stochastic processes underlying the cooperative switch of the motor can be obtained by analyzing the CCW and CW interval distributions [4,5,13]. We plot in Fig. 1 the probability density functions of CCW and CW intervals obtained from motors with the same CW bias ranging from 0.1 to 0.9. This approach contrasts with previous studies that combined CCW (CW, respectively) intervals from motors with different CW bias [6,9,14]. We found that the CW and CCW distributions are identical when the CW bias is equal to 0.5 and evolve antisymmetrically from this point. The CW and CCW distributions could be fitted with the gamma distribution function defined as

follows:

$$G_r(\tau) = \frac{\nu^r \tau^{r-1} \exp(-\nu\tau)}{\Gamma(r)},$$

where r and ν are, respectively, the shape and the scale parameter, and $\Gamma(r)$ the gamma function. The fit parameter r and ν are plotted as a function of the CW bias (Fig. 2). The r parameter represents the number of hidden steps of a Poisson process preceding the motor switch and occurring with the rate ν. Consequently, the mean duration of CCW (CW, respectively) time interval is given by the ratio r/ν (r'/ν', respectively). Since r in the gamma distribution represents the number of underlying Markov steps, r is chosen to be an integer. The rate ν is then equal to r divided by mean duration of the CW intervals. When the value of the parameter r saturates for both CCW and CW intervals, the maxima of the distributions are close to the resolution time of 0.1 sec of the experimental apparatus (CCW at high bias and CW at low bias). At this saturation level, the gamma distribution function fits well both CW and CCW interval distribution when the parameter r ranges from 4 to 5. We chose to perform arbitrarily the fits with $r = 5$ at the saturation level.

Power spectrum analysis.—Figure 3 shows averaged power spectra associated with binary time series collected from individual motors for a fixed value of the CW bias (i.e., [CheY*] level). Most of the spectra have a well-defined peaking frequency at $\sim 1~\text{s}^{-1}$. For CW bias = 0.1 the associated spectrum is almost flat with weak power amplitude at the peaking frequency. For larger CW bias the amplitude of the power at the peaking frequency increases reaching the maximum for CW bias = 0.5. After this point the amplitude of the power at the peaking frequency decreases with the CW bias. For a bias = 0.9, the shape of the
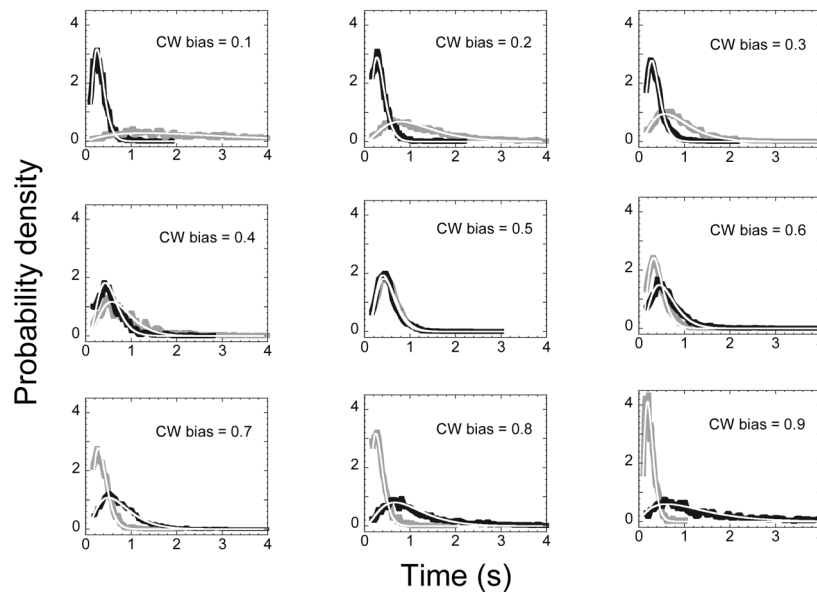

FIG. 1. Probability density functions of CCW (gray) and CW (black) time intervals as a function of CW bias. The bin size is 0.1 sec. Fit with gamma distribution function (white lines).
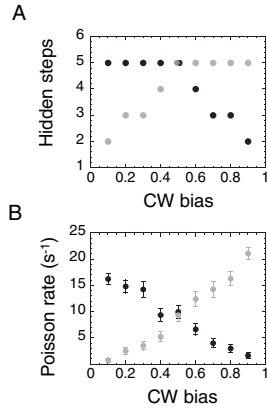
A

B

FIG. 2. Gamma distribution parameters as a function of the motor bias obtained from the fit of CW (black) and CCW (gray) distributions in Fig. 1. (a) Shape parameter, r, of the gamma distribution represents the number of hidden steps of a Poisson process, (b) Poisson rate (scale parameter, ν). The error bars represent the standard deviation due to differences in CW bias between cells within the same CW bias interval.

power spectrum is similar to that found for a CW bias = 0.1. At time scales larger than 1 s, the power spectrum exhibits a flat profile. It was shown analytically that the noise spectrum of a closed system of hidden reactions can exhibit "peaking" [16]. Similarly, the observed peaking of the power spectrum associated with the binary time series can be interpreted as the result of a hidden chain of Poisson steps preceding a switch. By contrast, if a switch were preceded by only one Poisson step ($r = 1$), then the CCW or CW intervals would be exponentially distributed and the associated power spectrum would be described by a standard Lorentzian. In the symmetrical case, when CW and CCW intervals are identically distributed, the amplitude of the power at the peaking frequency grows with the number of hidden Poisson steps [17]. We derive the expression of the autocorrelation function $B(\tau)$ following the same ap-
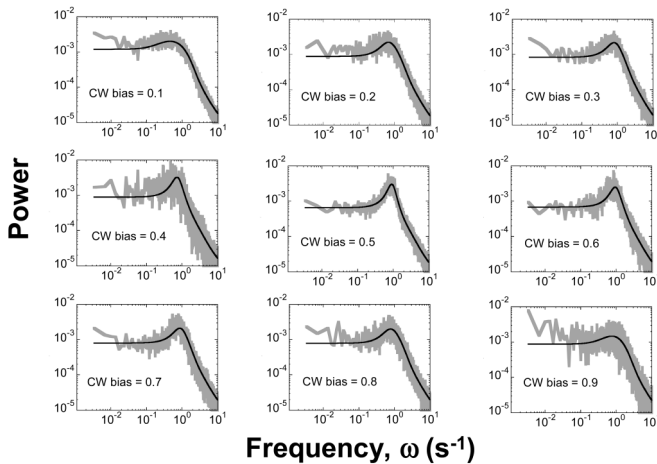

FIG. 3. Spectral characteristics of individual bacterial motors as a function of the CW bias (gray). Power spectra (black line) associated with simulated binary time series generated from gamma distributions.

proach as in [17], where $P_{01}(\tau)$ is the conditional probability for the system to be in state 1 at time $= \tau$ given that it was in state 0 at time $= 0$. Likewise, $P_{10}(\tau)$ is the conditional probability to be in state 0 at time $= \tau$ given that the state was 1 at time $= 0$. r and ν are the number of steps and Poisson process rate for the state 0 (CCW state), and r' is number of hidden steps and ν' is the rate of the Poisson process occurring in state 1 (CW state). G_n is the gamma distribution and $P_n = \frac{(\nu\tau)^n \exp(-\nu\tau)}{n!}$ is the Poisson probability. Similarly, G'_n and P'_n are functions of the rate ν'. In [17], the autocorrelation function was derived for symmetrical binary time series with identically distributed CCW and CW intervals.

$$B(\tau) = 1 - P_{01}(\tau) - P_{10}(\tau)$$

$$= 1 - \sum_{n=0}^{\infty} \left[\frac{1}{r} \sum_{i=1}^{r} \sum_{j=0}^{r'-1} \int_0^{\tau} G_{i+rn}(\tau_1) P'_{r'n+j}(\tau - \tau_1) d\tau_1 \right.$$

$$\left. + \frac{1}{r'} \sum_{i=1}^{r'} \sum_{j=0}^{r-1} \int_0^{\tau} G'_{i+r'n}(\tau_1) P_{rn+j}(\tau - \tau_1) d\tau_1 \right].$$

In our study, we derived the autocorrelation functions for nonsymmetrical binary time series using two distinct pairs of parameters taken from Fig. 2: (r, ν) for the gamma distribution of CCW intervals and (r', ν') for the gamma distribution of CW intervals [12]. The associated power spectra were obtained numerically using the Wiener-Khinchin theorem, and were plotted with the experimental spectra for various pairs of the r and ν parameters (Fig. 3). We found that the power spectra generated numerically reproduce well the profile of the experimental power spectra. This result suggests that the observed peaking frequency in the power spectra is caused solely by the nature of the distribution and not by the temporal correlations between the time intervals. To confirm the latter hypothesis, we found that the power spectrum profile with a peaking frequency was conserved when the experimental CCW and CW were randomly shuffled (data not shown).

Discussion.—By definition of the gamma function, the parameters r and ν are, respectively, the number of hidden Poisson steps occurring at a rate ν, which precedes a motor switch. Our analysis with the gamma distribution function suggests that each motor switch is preceded by several hidden Poisson steps. The standard assumption derived from simple two-state kinetic models was that the distribution of motor waiting intervals is exponential [6,14]. This assumption would imply that only one Poisson step precedes a motor switch. Under this condition, the associated power spectrum would exhibit a Lorentzian profile with no peaking frequency. Alternatively, we tested the model developed by Duke *et al.* [4]. In this stochastic model the conformational change of one subunit spreads through an idealized ring of closely packed subunits to mediate a switch. Each subunit has two conformations, active and inactive. If the whole ring is in the active
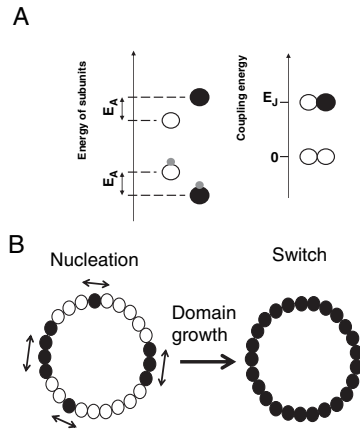
A

B

FIG. 4. (a) Energy diagram for motor subunits. White circle represents the inactive conformation; black circle is the active conformation of a subunit. Grey small circles are ligand molecules. The diagram is taken from [4] where $2E_J$ is the cost for creating two interfaces, and E_A is the energy difference between the active and inactive state of one subunit. (b) Domain growth of the ring of the motor. An idealized ring is represented by adjacent circles (subunits). Birth and growth of active domains (left), domains encompassed the whole ring (right).

(resp. inactive) conformation the motor rotates in the CW (resp. CCW) direction and maintains this direction until the whole ring switches to the inactive (resp. active) conformation. The intermediate states of the ring are composed of a mixture of active and inactive subunits and are *hidden* in this process because they do not cause a change of direction. Each nucleation event is associated with an energy change (ΔE) equal to either ($-E_A + 2E_J$) or ($E_A + 2E_J$); $2E_J$ is the cost for creating two interfaces, and E_A is the energy difference between the active and inactive state of one subunit [Fig. 4(a)]. In the Duke model the switching kinetics is mostly governed by a very strong coupling (E_J) between subunits where only one nucleation event induces a switch. If a motor switch was associated with the crossing of one energy barrier only, the power spectrum would exhibit a Lorentzian profile [18] with no peaking frequency, which is contrary to our experimental results. By contrast, in the regime of weak coupling (smaller E_J) but stronger E_A than in Duke *et al.*, several nucleation events can precede a switch. In this qualitative picture, we propose that the number of hidden steps is the number of nucleation events preceding a switch. The probability that the binding of one CheY* molecule induces one nucleation is a *fixed* characteristic of the motor and behaves like $\sim \exp(-\Delta E/kT)$. The probability that CheY* binds one subunit of the motor increases with the concentration [CheY*]. Therefore, the number of nucleation events per unit of time, ν, is proportional to $\exp(-\Delta E/kT)$, and increases with [CheY*] (i.e., CW bias) [Fig. 2(b)]. At higher CW bias (higher [CheY*]), the ring of protein subunits is bombarded by CheY* molecules with a higher rate yielding a greater number r of independent nucleation events [Fig. 2(a)]. Each nucleated domain will spread and

will combine together to encompass the whole ring after a time interval of about $\sim r/\nu$ [Fig. 4(b)]. Since the ring has a finite size, the number of nucleation events reaches saturation [Fig. 2(a)]. After the rth nucleation event, a switch occurs and then, a new series of hidden Poisson steps (nucleation events) starts all over with a different rate ν'. After a switch occurs the active (CW) ring can experience nucleation events again with a consecutive growth of the inactive domain and the motor switches back to the inactive (CCW) state. In the CW state, unoccupied active subunits are more likely to undergo a conformational change than occupied active subunits [see energy diagram Fig. 4(a)]. For this reason the nucleation rate ν' will decrease with the CW bias (i.e., [CheY*]) as depicted in Fig. 2(b).

In light of this discussion, it has become clear that we need new models that will incorporate all the characteristics of this large allosteric system. However, we interpreted the presence of a peaking frequency in the power spectrum as the consequence of a number of hidden Poisson events. Although there may exist other underlying mechanisms than the gamma distribution function to describe our data, experimental parameters such as the observed peaking frequency impose new strong constraints on any stochastic models of large individual allosteric complexes [4,5,10].

[1] H. C. Berg, Phys. Today **53**, No. 1, 24 (2000).
[2] P. Cluzel, M. Surette, and S. Leibler, Science **287**, 1652 (2000).
[3] T. Emonet *et al.*, Bioinformatics **21**, 2714 (2005).
[4] T. A. Duke, N. Le Novere, and D. Bray, J. Mol. Biol. **308**, 541 (2001).
[5] W. Bialek and S. Setayeshgar, Proc. Natl. Acad. Sci. U.S.A. **102**, 10 040 (2005).
[6] B. E. Scharf *et al.*, Proc. Natl. Acad. Sci. U.S.A. **95**, 201 (1998).
[7] J. Monod, J. Wyman, and J. P. Changeux, J. Mol. Biol. **12**, 88 (1965).
[8] D. E. Koshland, G. Nemethy, and D. Filmer, Biochemistry **5**, 365 (1966).
[9] U. Alon *et al.*, EMBO J. **17**, 4238 (1998).
[10] Y. H. Tu and G. Grinstein, Phys. Rev. Lett. **94**, 208101 (2005).
[11] E. Korobkova *et al.*, Nature (London) **428**, 574 (2004).
[12] E. Korobkova, Ph.D. thesis, University of Chicago, 2004.
[13] D. Bray and T. Duke, Annu. Rev. Biophys. Biomol. Struct. **33**, 53 (2004).
[14] S. M. Block, J. E. Segall, and H. C. Berg, J. Bacteriol. **154**, 312 (1983).
[15] S. C. Kuo and D. E. Koshland, J. Bacteriol. **171**, 6279 (1989).
[16] Y. Chen, J. Theor. Biol. **55**, 229 (1975).
[17] D. J. Odde and H. M. Buettner, Biophys. J. **75**, 1189 (1998).
[18] R. J. Glauber, J. Math. Phys. (N.Y.) **4**, 294 (1963).